Springer

KSME

Journal of Mechanical Science and Technology 31 (4) (2017) 1645~1655
www.springerlink.com/content/1738-494x(Print)/1976-3824(Online)
DOI 10.1007/s12206-017-0312-0

Investigation on aerodynamics and active flow control of a vertical axis wind turbine with flapped airfoil †

Yang Yang[1], Chun Li[1,2,*], Wanfu Zhang[1,2], Xueyan Guo[1,2] and Quanyong Yuan[1]

[1]*School of Energy and Power Engineering, University of Shanghai for Science and Technology, Shanghai, 200093, China*
[2]*Shanghai Key Laboratory of Multiphase Flow and Heat Transfer in Power Engineering, Shanghai 200093, China*

(Manuscript Received May 23, 2016; Revised October 19, 2016; Accepted December 5, 2016)

Abstract

A 2D unsteady numerical simulation with dynamic and sliding meshing techniques was conducted to solve the flow around a three-blade Vertical axis wind turbine (VAWT). The circular wakes, strip-like wakes and the shedding vortex structures interact with each other result in an extremely unstable performance. An airfoil with a trailing edge flap, based on the NACA0012 airfoil, has been designed for VAWT to improve flow field around the turbine. Strategy of flap control is applied to regulate the flap angle. The results show that the flapped airfoil has an positive effect on damping trailing edge wake separation, deferring dynamic stall and reducing the oscillating amplitude. The circular wake vortices change into strip vortices during the pitch-up interval of the airfoils. Examination of the flow details around the rotating airfoil indicates that flap control improves the dynamic stall by diminishing the trend of flow separation. Airfoil stall separation has been suppressed since the range of nominal angle of attack is narrowed down by an oscillating flap. Vortices with large intensity over rotational region are reduced by 90 %. The lift coefficient hysteresis loop of flapped airfoil acts as an O type, which represents a more stable unsteady performance. With flap control, the peak of power coefficient has increased by 10 % relative to the full blade VAWT. Obviously, the proposed flapped airfoil design combined with the active flow control significantly has shown the potential to eliminate dynamic stall and improve the aerodynamic performance and operation stability of VAWT.

Keywords: Aerodynamics; Control strategy; Flapped airfoil; Vertical axis wind turbine (VAWT)

1. Introduction

Wind power is one of the most promising and sustainable energy sources due to the concerns on worsening environmental pollutions, the increasing energy requirements and fossil fuel depletion [1, 2]. Lift-type wind turbine is the most popular device for extracting wind energy. It can be divided into Horizontal axis wind turbine (HAWT) and Vertical axis wind turbine (VAWT) by the position of the rotational axis. Fig. 1 shows the difference of forces and velocities acting on HAWT and VAWT for various azimuthal positions.

The pressure and suction surfaces of VAWT blade are in alternative variation during a rotation cycle. The natural structural features resulting in the variation of angle of attack (α) for VAWT blade are very different from HAWT blade. A significant changing of angle of attack leads to unstable aerodynamic performance. It is the primary reason that VAWT is considered to have a lower power coefficient than HAWT. The importance of VAWT has long been ignored and underestimated. In the next 20 or 30 years, the power coefficient of VAWT is expected to be equal or higher than that of HAWT due to the development of lift-type wind turbine. Furthermore,

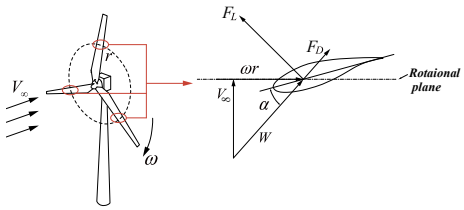

(a) HAWT

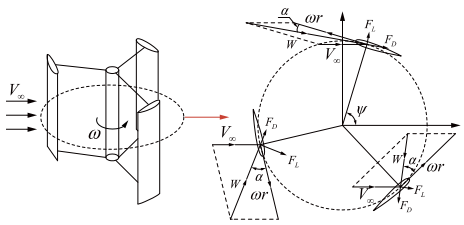

(b) VAWT

Fig. 1. Forces and velocities acting on HAWT and lift-type VAWT for various azimuthal positions.

*Corresponding author. Tel.: +86 21 55271729, Fax.: +82 21 55271729
E-mail address: lichun_usst@163.com
† Recommended by Associate Editor Kyu Hong Kim

VAWT has some natural advantages over HAWT because of its low maintenance, simple blade structure, low construction cost and no yawing. VAWT will play an important role in future wind power [3, 4].

However, angle of attack for blades of a VAWT changes significantly during its rotation cycle, and these changes lead to serious flow separation and dynamic stall when the angle of attack is sufficiently large in some phase positions. Flow separation and dynamic stall will subsequently result in substantial instability of aerodynamic loads on the blades and induce vibration and noises. The power and aerodynamic efficiency of a VAWT are thus significantly influenced [5, 6]. Therefore, an in-depth investigation of the aerodynamic performance of VAWTs is necessary and important.

The trailing edge flap of a helicopter is normally applied as a reference for wind turbine blade due to their similar structure. Friedmann et al. [7] studied vibration reduction of the trailing edge flap of a helicopter at both high and low speed flight mode. Results indicate that hub shear force and momentum can be reduced substantially by an actively controlled flap. Viswanurthy et al. [8] reduced the vibration of helicopter rotors with multiple trailing edge flaps. Results indicate that multiple trailing edge flaps have a good ability to reduce vibration under low driving power. Maucher [9] reached similar conclusions that vibration and noise of helicopter can be effectively reduced by continuous deformation trailing edge flap. Msihra et al. [10] applied the Computational structural dynamics (CSD) coupled method to analyze the effect of trailing edge flaps on vibration reduction of helicopter and they found load reduction in the hub.

The working condition for a helicopter is different from a wind turbine and should be modified. Bossanyi [11] proved that the pitch load on each blade can be alleviated individually by adjusting the pitch angle. Larsen [12] proposed a new strategy for individual pitch control. The blade pitch angle was adjusted based on the attack angle and relative velocity of incoming flow. Simulation shows that 25 % of fatigue load can be reduced in out-of-plane direction. Buhl et al. [13] established a two-dimensional aero-elastic model by using potential flow theory and investigated the load reduction ability of the trailing edge flap. They concluded that the trailing edge flap has the ability to reduce fluctuating loads significantly, but the effect varies with the incoming flow. Barlas et al. [14] studied the influence of active flap control on the 5MW upwind wind turbine; 16 % to 22 % load reduction can be achieved by using trailing edge active flow control. Andersen [15] designed a control strategy of full scale blade and also combined dynamic stall model and near-field and far-field wake model with traditional potential flow theory. The results show that three trailing edge flaps on each blade of 5MW HAWT could decrease 60 % of out-of-plane direction fatigue momentum. In addition, he also found that the type of trailing edge flap and controlling strategy have different load reduction effects. Lackner [16] analyzed the load reduction capabilities of trailing edge flap and individual pitch control by XFOIL and GH Bladed. Results show that the individual pitch control is better for low frequency load while the trailing edge flap is more suitable for high frequency load. Markou et al. [17] studied the impacts of individual pitch control, and a trailing edge flap on downstream wake reduction of wind turbine and trailing edge flap had better effectiveness on load reduction.

In terms of flap aerodynamic performance, different flap parameters can be optimized based on their flow field structure in the CFD modelling. Zhu et al. [18] applied immersed boundary technique to investigate aerodynamic performance of 2D airfoil with deformable trailing edge. The obtained results show that the approach is efficient and accurate for simulating turbulent flow around airfoils with a trailing edge flap. Lutz et al. [19] designed a rigid trailing edge flap based on NACA 64618, which had a length of 10 % chord length by using XFOIL. CFD solver FLOWER was applied to check the aerodynamic performance of an airfoil with movable flap. The lift coefficient can be changed by the rigid trailing edge flap to a certain extent. Troldborg [20] used the CFD simulation to compare aerodynamic performance of trailing edge flap with different geometries. The results reveal that moderate bending flap has both better aerodynamic performance and ability to control flow separation than the rigid large bending flap. Tan et al. [21] employed PIV measurement to prove the ability of a flap to change vortex development around the airfoil. Xiao et al. [22] explored the potential of fixed and oscillating flap to improve flow field around vertical axis tidal turbine. The results show that a flap could increase the power coefficient of a turbine and delay stall under large angle of attack.

Previous studies mainly focus on control strategy and load reduction of helicopter and HAWT. The investigation on trailing edge flap applied on VAWT is rare. In addition, stall vortex structure around a wind turbine blade with trailing edge flap is not fully understood.

In the present work, an airfoil with a trailing edge flap was designed for a VAWT, and the dynamic aerodynamic performance of the VAWT was analyzed by numerical simulation. Based on the characteristics and vortex structures of the resolved unsteady flow field, a control strategy of flap deflection is proposed for deferring the dynamic stall of the VAWT and efficiently reducing the aerodynamic load on the blades.

2. The numerical model

2.1 The physical model

Since each blade of a VAWT experiences opposite phase positions in the two halves of the cycle perpendicular to the incoming flow when the VAWT rotates, a symmetric NACA0012 airfoil was chosen as the base airfoil, whose chord length CAB = 50 mm. At the point 1/4 CAB from the trailing edge point B, a flap was placed, with a length of 1/4 C, as illustrated in Fig. 2. The gap between the flap and the main airfoil was 1/30 C.

The flap was allowed to swing or deflect around point O in

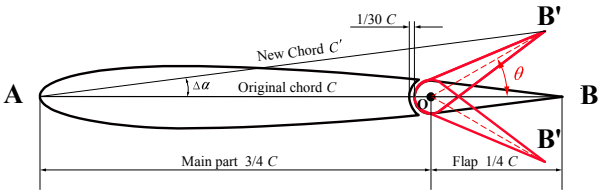

Fig. 2. Schematic diagram of the airfoil with flap.

a range of $\pm 30°$. The angle between the original flap chord OB and the OB' (connection of rotation center O and the deflected trailing edge point B'). θ was defined as the flap angle. A positive θ was defined when the flap swings counterclockwise in Fig. 1. Changing the flap angle changes the chord of the airfoil and then the angle of attack of the airfoil, leaving the leading edge position unchanged. Relative to the original chord AB, AB' is the nominal chord and the angle formed by AB and AB' is the angle of attack $\Delta\alpha$, which can be determined as a function of θ as follows,

$$\Delta\alpha = \frac{d\alpha}{d\theta} = \arctan\left(\frac{\sin\theta}{3+\cos\theta}\right). \quad (1)$$

2.2 The computation domain and its meshing

A C-shaped domain (ABCEFG) is chosen for the 2D simulation of the VAWT, as shown in Fig. 3(a). The diameter of the wind turbine is D = 1200 mm, which is one-fifth of the diameter of the region of incoming flow (the half circle AFG). The squared downstream region (ABCEF) is 10D to ensure a full development of wakes. The domain consists of three subdomains: internal zone (Zone 1), rotating zone (Zone 2) and external zone (Zone 3). The three zones are connected by interfaces which are used to merge separate computation domains into a single and continuous one, as illustrated by the dashed lines. In zone 2, unstructured triangular mesh was applied since the control strategies of swinging flaps are applied and thus dynamic remeshing is required. Structured meshing was used for zone 1 and zone 3, in which meshes in areas around the airfoils and shaft were locally refined to follow the high gradients. Fig. 3(b) shows the representative meshing details of the computation domain. Sliding meshing was used to couple the rotating zone 2 and the stationary zone 3, and dynamic meshing was applied to handle the swinging flaps in zone 2. The total grid size of the computation domain is 530000 and the time step size is 2.6×10^{-4} s, with 3600 time steps in a rotation cycle.

The physical properties as density and dynamic viscosity are $\rho = 1.225$ kg/m^3 and $\mu = 1.7894\times10^{-5}$ kg/(m·s), respectively. Incoming velocity, Reynolds number and Mach number were chosen as $V = 10$ m/s, $\mathrm{Re} = 6.85\times10^5$, and $Ma = 0.03$. In the computation domain, a constant velocity was chosen on the boundaries AED, AB and DE, as velocity inlet boundary condition, and a constant pressure on the boundary BD as the pressure outlet boundary condition, with non-slip on the airfoil walls. ANSYS Fluent® was chosen to solve the

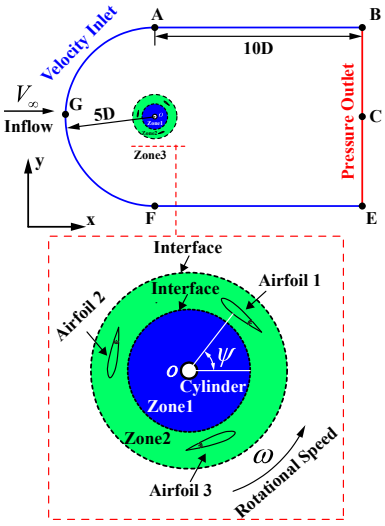

(a) Calculation field

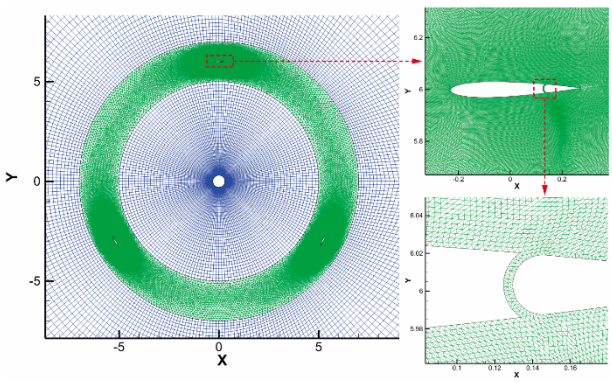

(b) Grid distribution

Fig. 3. Calculation field and grid distribution.

unsteady Reynolds averaged Navier-Stokes equations (RANS), with the finite volume method SIMPLE , the turbulent model S-A, and the standard wall function were chosen as the sub setting.

Angle of attack is one the most important design parameters for wind turbines. In a rotation cycle, the angle between airfoil 1 and the positive x axis in the coordinates system is defined as the azimuth angle ψ shown in Fig. 2(a), and the angle between incoming velocity V_∞ and the nominal chord AB' shown in Fig. 2 is defined as the nominal angle of attack α. When flap angle $\theta = 0°$, the angle of attack α_0 is defined as initial angle of attack. For a given tip-speed ratio λ, the initial angle of attack α_0 is a function of the azimuth angle ψ and the tip-speed ratio λ as follows,

$$\alpha_0 = \arctan\left(\frac{\cos\psi}{\lambda+\sin\psi}\right). \quad (2)$$

For VAWTs, large tip-speed ratio does not always determine better performance. Fig. 3 shows power coefficient C_p changes with tip-speed ratio at different solidity [23]. It can be found that C_p increases with λ first and then decreases with

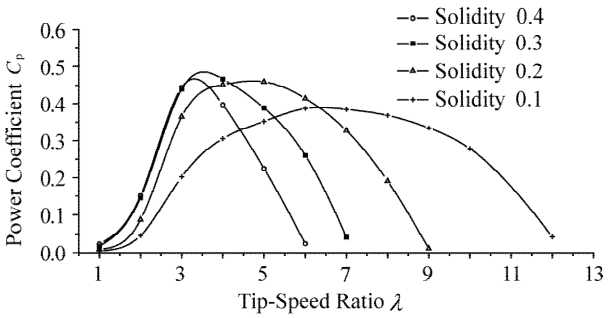

Fig. 4. Power coefficient vs. tip-speed ratio at different solidity.

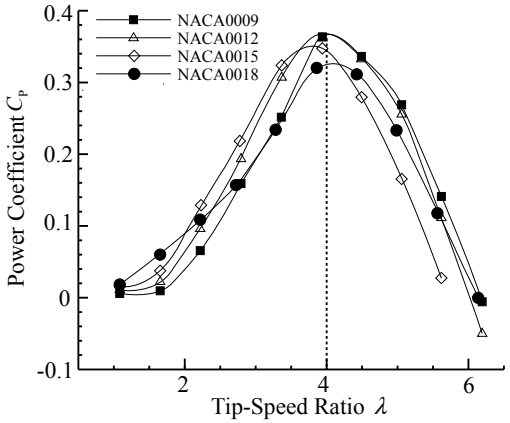

Fig. 5. Wind power coefficient vs. tip-speed ratio for different thickness airfoil.

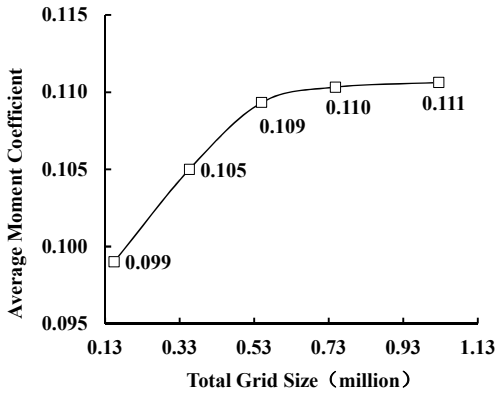

Fig. 6. Grid independence.

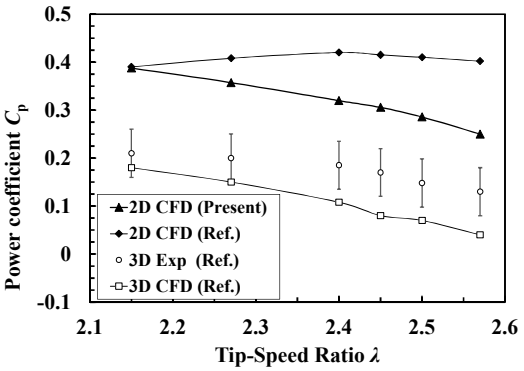

Fig. 7. Comparison of present numerical result and reference results.

maximum C_p changing with solidity. The maximum C_p is reached at $\lambda = 3.5$ for a solidity of 0.2 and at $\lambda = 4.5$ for a solidity of 0.3. In the present case, the blade chord is 50 mm and rotor diameter is 1200 mm. The solidity is 0.25. The design tip speed ratio is set to 4 to reach the maximum C_p.

Fig. 5 shows C_p changes with the tip-speed ratio at different NACA airfoils. It turns out that C_p increases with the increase of tip-speed ratio and then decreases with the increase of tip-speed ratio, with the maximum C_p being reached at $\lambda = 4$. C_p even turns negative when tip-speed ratio is over 6. Here, NACA0012 is selected as baseline airfoil.

For $\lambda = 4$, the nominal angle of attack can be finally obtained as a function of azimuth angle and flap angle:

$$\alpha = \alpha_0 + \triangle\alpha = \arctan(\frac{\cos\psi}{4+\sin\psi}) + \arctan(\frac{\sin\theta}{3+\cos\theta}) . \quad (3)$$

3. Results and discussion

3.1 Grid independence and validation of numerical simulation

To verify the validity of this present study, the results of numerical simulation and experimental measured in Ref. [2] are chosen for comparison. Grid independence is the first step. For that tested VAWT, mesh refining is carefully conducted near the airfoil walls with five different orders for the height of the first grid cells near the wall. The moment coefficient C_M is sensitive to the near-wall gridding and the total grid size. Fig. 6 shows the average moment coefficient during rotational cycle. The coarsest grid yields a deviation of 10.8 % compared with finest one. It seems that the medium size (550000) is acceptable and used in the simulation as its deviation is only 1.80 %. The height of the first grid cell near the wall is 1.0×10^{-4} m.

According to the tested conditions, the tip speed ratios are, respectively, 2.15, 2.27, 2.40, 2.50 2.55 and 2.60, with the inflow velocity 5.07 m/s. The comparison with reference results is shown in Fig. 7. The power coefficient versus tip speed ratio of the present study has the same variation tendency as reference 3D numerical simulation and experimental measured results. Present study produced a lower deviation of power coefficient than that of reference 2D numerical simulation in all tested conditions. The grid distribution and turbulent model appears to be acceptable.

3.2 Dynamic aerodynamic characteristics (Without flap control)

As a reference case, flow field and dynamic aerodynamic characteristics for the VAWT without flap control (flap angle $\theta = 0°$) are first discussed. For a clear description of the movement and the phase positions of the blades of VAWT,

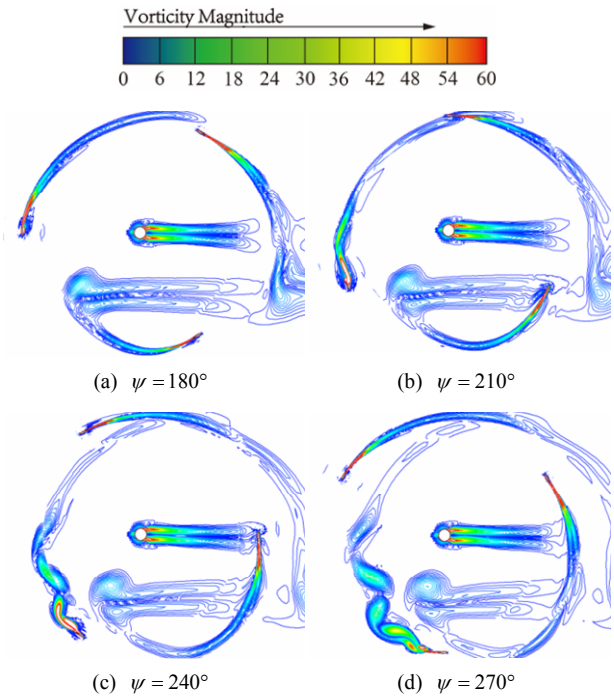

Fig. 8. Wake evolution during the first cycle.

the pitch-up movement is defined when the nominal angle of attack α increases, and the pitch-down movement when α decreases. When the tip-speed ratio $\lambda = 4$, the pitch-down phase corresponds to the range of azimuth angle $-14.5° < \psi \le 194.5°$, and the pitch-up phase corresponds to the range of $194.5° < \psi \le 346.5°$.

Since the pitch angle is 120° for a three-blade VAWT, a 1/3 cycle can describe flow characteristics of the full cycle. With an interval of 15° of azimuth angle, the vorticity distribution of the first rotation cycle is shown in Fig. 8. This illustrates clearly how the wakes form, evolve and interact behind the blades and the shaft. The wakes behind the blades start to interact at $\psi = 180°$, as in Figs. 8(a) and (b), and then fully interact after the azimuth angle is larger than 240°, as in Figs. 8(c) and (d). Obviously, the flow field is very complicated in the last 1/3 cycle and the blades basically move in the wakes of the blades in front of it.

In Fig. 9, vorticity contours are displayed for $\psi = 90°$ in the third and fourth cycle. The wake structures and their evolution are substantially similar in the two cases, from which we can conclude that a stable flow pattern has been established and typical flow phenomena and structures have emerged. There are three typical wake structures, which we define as S_1, S_2 and S_3, respectively. S_1 wake vortices appear usually during the pitch-up period in a rotation cycle of the VAWT, flow structures contain mainly circular spots or areas with larger vorticity. S_2 wake vortices contain strip-like areas of larger vorticity and exist during the pitch-down period in a rotation cycle. S_3 wakes mainly form and evolve behind the shaft, with vortices shedding, which belongs to Karman vortex

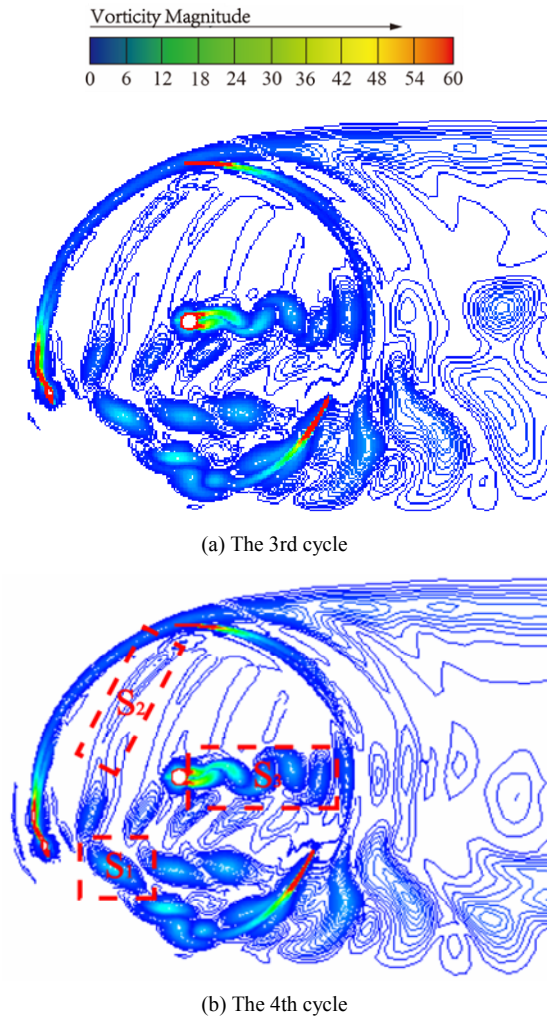

Fig. 9. The wake vortex structures in the flow field (in the 3rd and 4th cycles).

street. In their downstream area, the S_3 wakes also interact with the blades that pass by and the relevant wakes. After several cycles, the flow field looks complicated or even chaotic due to the strong interaction of the wakes from all the blades and the shaft.

To shed more insight on the flow fields around the airfoils, enlarged vorticity contour in areas surrounding the airfoils at various azimuth angles is shown in Fig. 10. Figs. 10(a), (c), (e) and (g) show the vorticity magnitude around the airfoil in pitch-up phase, whose nominal angle of attack are -14.4°, -11.2°, -3.4° and 6.4°, respectively. Figs. 10(b), (d), (f) and (h) show the vorticity magnitude under corresponding nominal angle of attack in pitch-down phase. In Fig. 10(a) the shedding vortices are circular and obviously characterized as a vortex structure of dynamic stall. The wakes then gradually evolve into the typical S_1 wakes. In Fig. 10(b), strip-like wakes are observed at the trailing edges of the airfoils, which are attached on the airfoil surfaces and finally develop into the S_2 wakes as displayed in Fig. 9(b). According to a comparison of

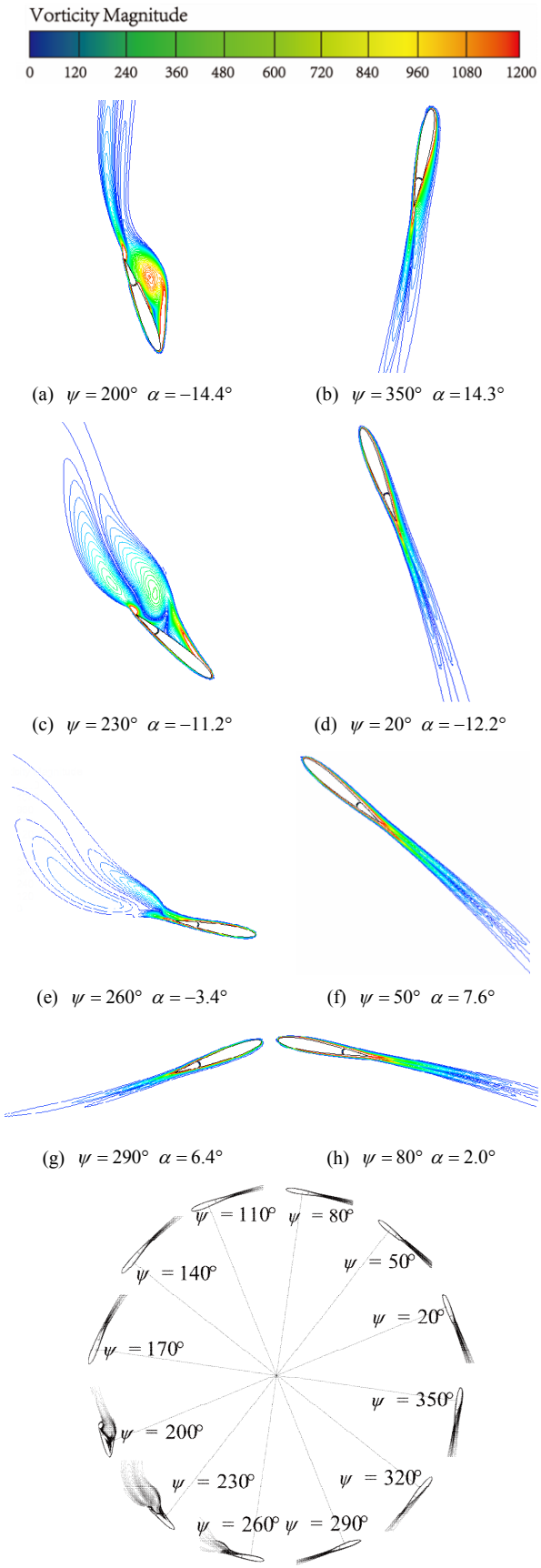

Fig. 10. The wake vortex structures around an airfoil.

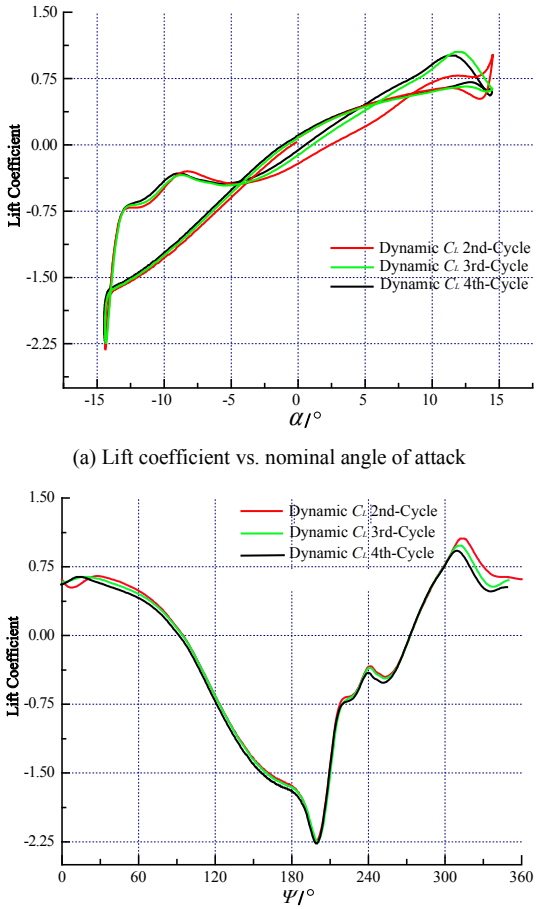

(a) Lift coefficient vs. nominal angle of attack

(b) Lift coefficient vs. azimuth angle

Fig. 11. Lift coefficient vs. angle of attack or azimuth angle.

the two cases discussed above, different wake vortex structures are found for the same nominal angle of attack of 14.4° but during the opposite phase positions: Pitch-up or pitch-down phases. In fact, the cycle phase, pitch-up or pitch-down, can be identified by watching the wake types: Circular wakes for pitch-up phase and strip wakes for pitch-down phase.

The structures of the wake vortices determine as well the aerodynamic coefficients like lift and drag coefficients, and the lift-drag ratio, which vary periodically along with the nominal angle of attack during the rotation of the VAWT.

Fig. 11 shows how lift coefficient changes during the rotation cycles. In Fig. 11(a), the maximum lift coefficient during pitch-up and pitch-down phases is different in the second, third and fourth cycles for the same α. Fig. 11(b) illustrates the azimuth angle at which the maximum lift coefficient is observed for the blades. During the pitch-up phase, a maximum lift coefficient of 0.94 is found at $\psi = 306°$, and a maximum value of 0.66 is found at $\psi = 15°$ in the pitch-down phase. Also, in Fig. 11(b) the lift-azimuth curve in pitch-down phase is much smoother than that in pitch-up phase although the latter exhibits a higher peak value. In fact, the wavy curve may imply complicated boundary layer transition or separation.

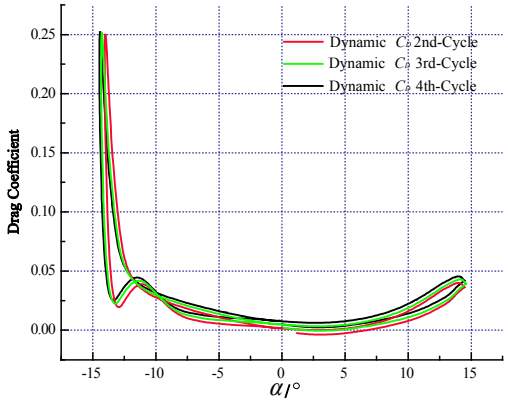

(a) Drag coefficient vs. nominal angle of attack

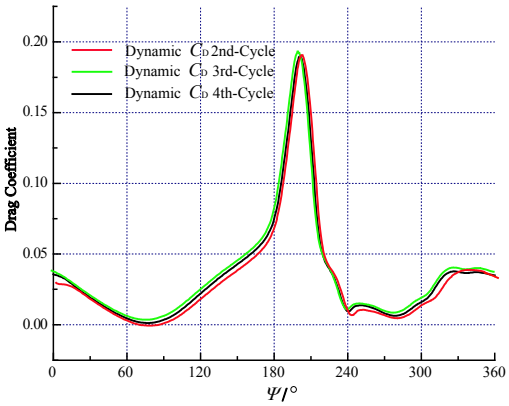

(b) Drag coefficient vs. azimuth angle

Fig. 12. Drag coefficient vs. angle of attack or azimuth angle.

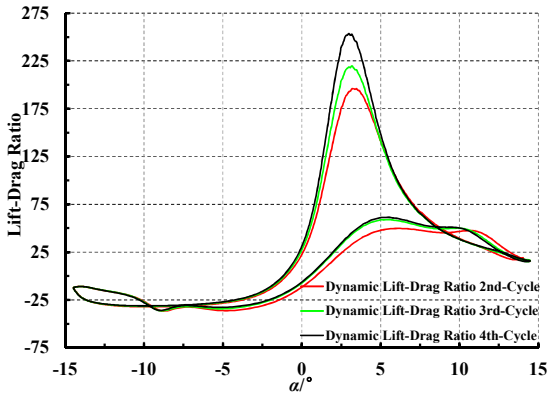

(a) Lift-drag ratio vs. nominal angle of attack

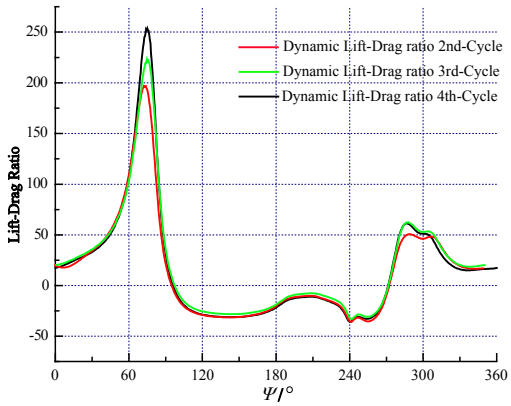

(b) Lift-drag ratio vs. azimuth angle

Fig. 13. Lift-drag ratio vs. angle of attack or azimuth angle.

In Fig. 12(a), the airfoil drag coefficient is plotted against the nominal angle of attack for three cycles. There is a sudden jump in the drag coefficient when the airfoil pitches down to a large angle of attack. This corresponds to strong vortices shed around airfoil according to Figs. 12(a) and (b). Fig. 12(a) also shows that drag coefficient remains lower than 0.05 in almost 90 % of the range of angle of attack. Variation of drag coefficient along with the azimuth angle is plotted in Fig. 12(b). The drag increases with the azimuth angle in the range $180° < \psi < 240°$. Although the lift coefficient reaches its maximum value in the same range of azimuth angle, the aerodynamic performance of the airfoil in the above range of azimuth angle is not soundly good. Therefore, lift-drag ratio may be a better parameter to evaluate the aerodynamic performance of an airfoil.

Fig. 13 illustrates the lift-drag ratio changes along with the nominal angle of attack or azimuth angle. In the pitch-up phase and with an increase in the nominal angle of attack, the lift-drag ratio increases first and then decreases. The maximum lift-drag ratio occurs at $\alpha = 4°$, which corresponds to $\psi = 70°$. By observing the vorticity contours in Fig. 10, the lift-drag ratio in pitch-down phase is obviously higher than that in pitch-up phase.

The changes of turbulent viscosity in the flow field around the airfoil in the fourth cycle are displayed in Fig. 14. The turbulent viscosity represents the existence of the wall induced vortices or eddies and its evolution displays the course of development of eddies in the flow field. Thus, the decrease in turbulent viscosity implies viscous dissipation. By comparing the two pairs of contours in Figs. 14(a) and (b), as well as in Figs. 14(c) and (d), time dependence of turbulent viscosity in two close phase positions ($\psi = 200°$ and $\psi = 210°$, $\psi = 280°$ and $\psi = 290°$) is observed. Obviously, eddies dissipate gradually and the dissipation in the strip wakes is much faster than in the circular wakes. In fact, the circular wake vortices generated by the pitch-up movement of airfoils evolve into very complicated vortex systems and last much longer.

3.3 Improvements of flow fields and aerodynamic performance

Based on a thorough understanding of the flow field around the VAWT and the aerodynamic characteristics of the VAWT, a flap control strategy was proposed to defer the dynamic stall of the VAWT and minimize the oscillation of the torque output of the VAWT.

The nominal angle of attack is plotted against the azimuth

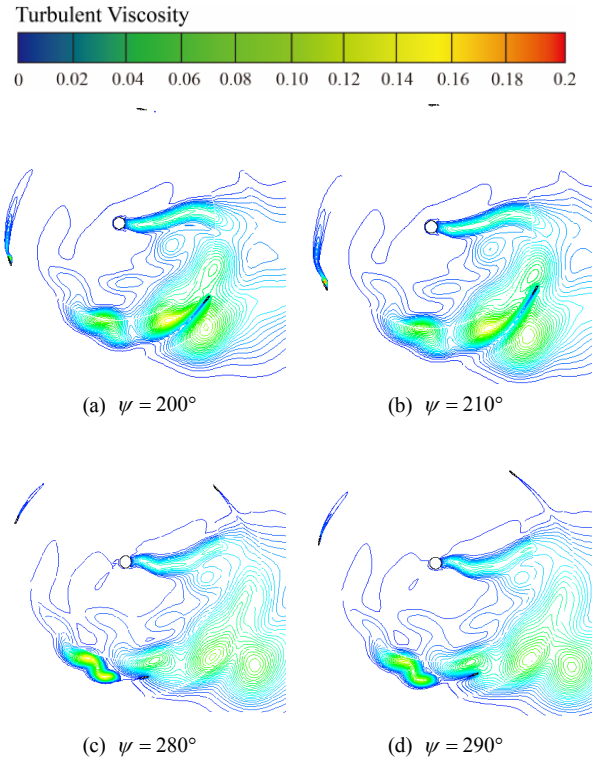

Fig. 14. Distribution of turbulent viscosity.

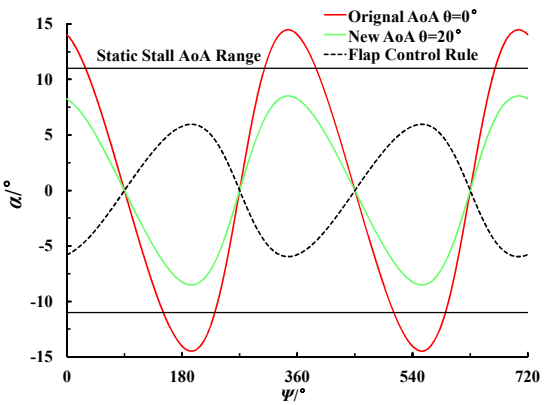

Fig. 15. Nominal angle of attack vs. azimuth angle.

angle in Fig. 15 based on Eq. (3). The maximum nominal angle of attack is ±14.5°, corresponding to the azimuth angle of $\psi = 193°$ and $\psi = 346°$, respectively. Since the static stall angle of attack for NACA0012 is ±11°, a factor $k(k < 0)$ is introduced to limit the flap angle θ, in order to finally control the nominal angle of attack in a safe range, i.e., $-11° < \alpha < 11°$, as in Eq. (4),

$$\theta = k[\tan^{-1}(\frac{\cos\psi}{4+\sin\psi})]. \quad (4)$$

As found in Fig. 13(a), a large lift-drag ratio for NACA0012 exists in a range of ±8.5° for angle of attack. When α is outside the range, the drag coefficient increases

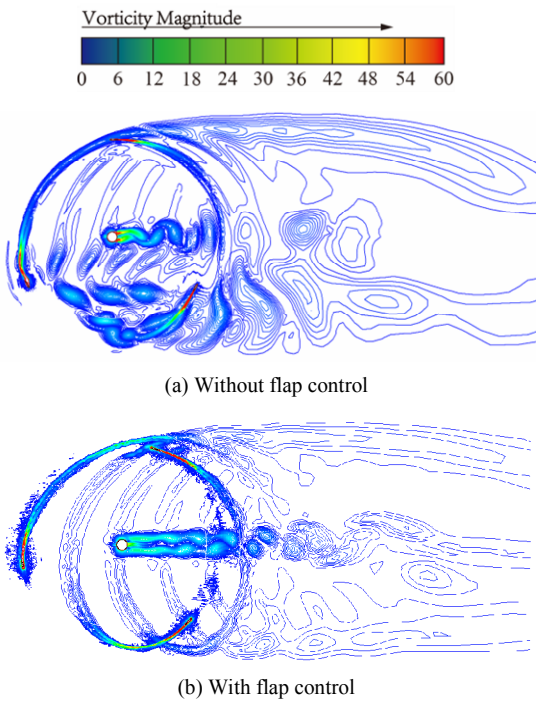

Fig. 16. Vorticity distribution: without and with flap control.

rapidly due to, probably, boundary layer transition or separation. In the present work, the factor k was chosen as k = -5/3, and the corresponding maximum flap angle θ is 20°.

The flap control strategy defined with Eq. (4) was coded in a User defined function (UDF) in the ANSYS Fluent solver to control the flap movement. Here, the azimuth angle is expressed with the angular velocity of the turbine ω as $\psi = \omega t$ and the temporal derivative of the flap angle is used to calculate the flap angle increment in each time step.

$$\theta' = k\frac{\omega[1+4\sin(\omega t)]}{17+8\sin(\omega t)}. \quad (5)$$

Fig. 16 shows the vorticity contour for the flow field around the VAWT, without and with flap control. It can be found that the wake vortex structures in the pitch-up phase have been substantially changed by the flap control, compared with the original case without flap control. The original circular wake vortices in pitch-up phase have almost turned into strip-like ones that usually exist in the pitch-down phase. The situation in pitch-down phase remains unchanged.

In Fig. 17, the vorticity distribution around an airfoil is displayed to compare how much the flap alters the nearby flow field around the airfoil. Here, the case without flap control at various azimuth angles is on the left and the one with flap control on the right. Flow separation almost occurs in the whole pitch-up phase, and results in the largest drag in a rotation cycle for the VAWT. With flap control, the airfoil operates completely outside the static stall range of angle of attack. Therefore, swing flap restrains the formation and development of wake vortices to a large extent, and this improves the flow

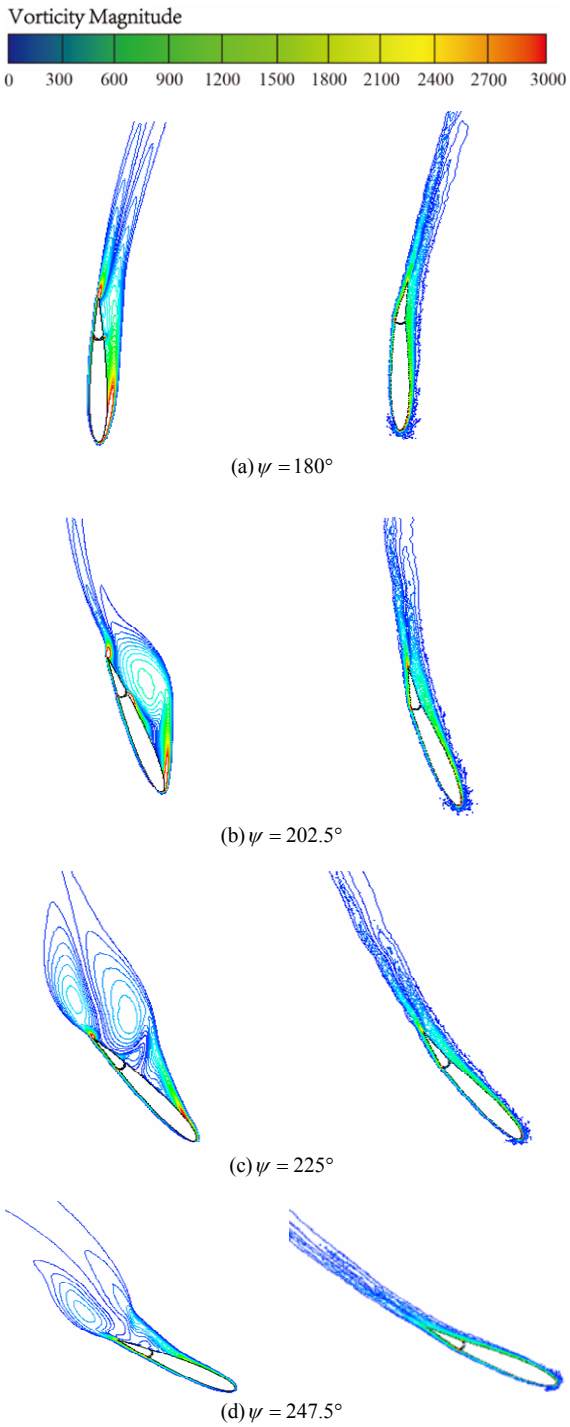

Fig. 17. Vorticity distribution in the nearby flow filed around the airfoil.

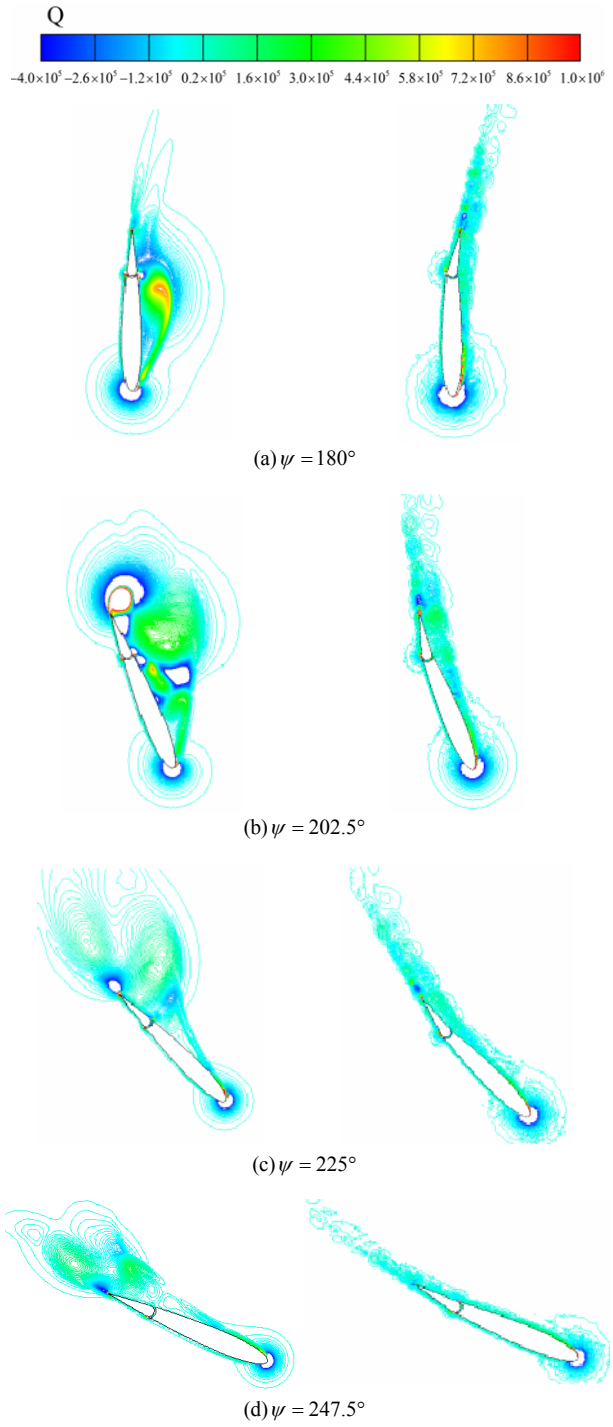

Fig. 18. Q-criterion distribution in the nearby flow field around the airfoil.

field substantially.

To demonstrate more details of the flow field, the Q-criterion contour around the airfoil is given in Fig. 18. The left and right columns represent airfoil without and with flap control, respectively. According to the definition of the Q-criterion [24], a large positive Q implies strong rotation and the strain and shear are overcome. On the other hand, the positive Q regions indicate the cores of vortices or turbulent structures. In Fig. 14, the Q-criterion for the case without flap control is often over 105, which means the existence of strong vortices around the airfoil. Opposite to that, smaller regions with lower Q are observed for the cases with flap control. Obviously, the flap control significantly hampers the formation and evolution of the vortices near the airfoils.

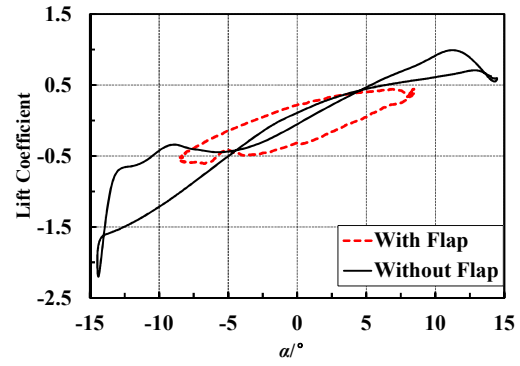

(a) Lift coefficient

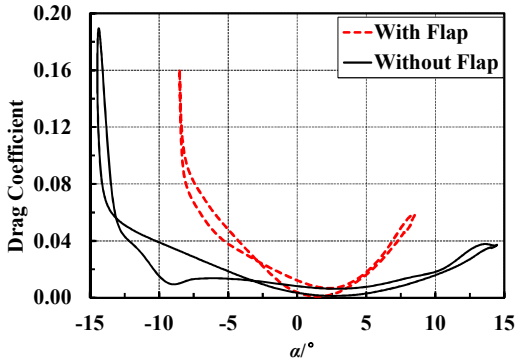

(b) Drag coefficient

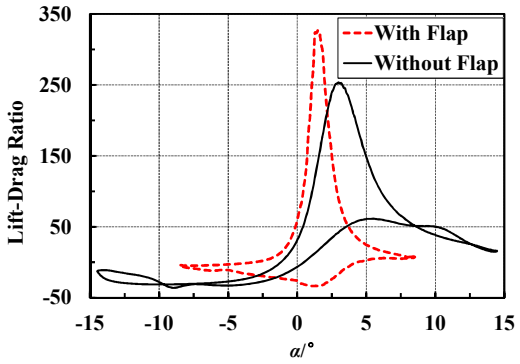

(c) Lift-drag ratio

Fig. 19. Aerodynamic performance of the flapped airfoil.

Fig. 19 shows a comparison of dynamic lift coefficient, drag coefficient and lift-drag ratio between flapped airfoil and normal airfoil. During a rotational cycle, the nominal angle of the attack range of a flapped airfoil is narrower than that of normal airfoil. The lift coefficient hysteresis loop for flapped airfoil is like an O type, which is significantly different from that of normal airfoil. The flapped airfoil has a more stable unsteady aerodynamics. The average lift coefficient and maximum lift-drag ratio increase 0.15 and 73, respectively. It indicates that the oscillating flap has a positive effect on aerodynamic performance of VAWT.

Fig. 20 shows the variation of power coefficient versus tip speed ratio for the VAWTs with and without flap control. Without flap control, the maximum power coefficient is

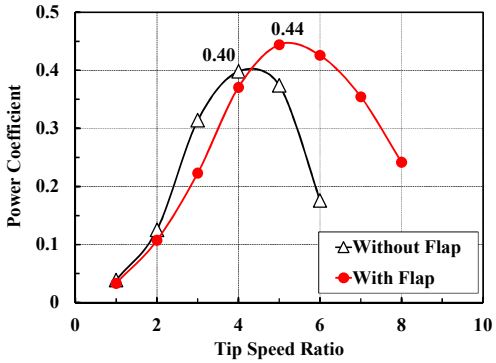

Fig. 20. Power coefficients versus tip speed ratio.

reached near a tip speed ratio equal to 4 as expected. With flap control, the maximum power coefficient is reached at a tip speed ratio of 5. The effect of flap control is negative for the efficiency of VAWT when the tip speed ratio is lower than 5. Although an oscillating flap improves the aerodynamic performance of the airfoil as shown in Fig. 19, the angle between the actual moment and effective moment has increased due to nominal angle of attack changed by flap oscillating. The overall efficiency of turbine failed to increase as expected in that condition. Along with the increasing of tip speed ratio, the power coefficient increases. The peak of power coefficient has increased by 10 % with flap control. The oscillating flap also widensthe effective operation region of VAWT.

4. Conclusions

An airfoil with a trailing edge flap, based on the NACA0012 airfoil, has been designed for VAWT. 2D unsteady numerical simulation with dynamic and sliding meshing techniques was conducted to solve the flow around a three-blade VAWT. The simulation indicates that there are mainly three types of wake vortex structures, including circular wakes, strip-like wakes and the shedding vortices similar to Karman vortex street. The three wake structures interact with each other and result in an extremely complex flow field.

Based on the simulation, an active flow control strategy of flapped airfoil was proposed to improve the dynamic stall and reduce the blade wake vortex interaction. Examination of the flow details around the rotating airfoil indicates that flap control improves the dynamic stall by diminishing the trend of flow separation. The oscillating flap narrows the range of nominal angle of attack. It is beneficial to suppress airfoil stall separation. The lift coefficient hysteresis loop of flapped airfoil acts as an O type, which represents a more stable unsteady performance. With flap control, the peak of power coefficient is increased by 10 % relative to the full blade VAWT.

The results of flapped airfoil performance and flow field around the turbine have shown the huge potential of oscillating flap to eliminate dynamic stall associated with VAWT blade. For further study, 3D numerical simulation of VAWT is recommended for analyzing the separated flow and wake of blade tip.

Acknowledgments

This research was financially supported by National Natural Science Foundation of China (grant numbers 51676131 and 11402148), Shanghai Science and Technology Commission Project (grant number 13DZ2260900). And the authors would like to give special thanks to Dr. Dunyu Liu, whose guidance and encouragement have been of great importance in achieving the present results.

References

[1] R. K. Singh, M. R. Ahmed, M. A. Zullah and Y. H Lee, Design of a low Reynolds number airfoil for small horizontal axis wind turbines, *Renewable Energy*, 42 (1) (2012) 66-76.

[2] R. Howell, N. Qin, J. Edwards and N. Durrani, Wind tunnel and numerical study of a small vertical axis wind turbine, *Renewable Energy*, 35 (2) (2010) 412-422.

[3] L. A. Danao, O. Eboibi and R. Howell, An experimental investigation into the influence of unsteady wind on the performance of a vertical axis wind turbine, *Applied Energy*, 107 (4) (2013) 403-411.

[4] S. Eriksson, H. Bernhoff and M Leijon, Evaluation of different turbine concepts for wind power, *Renewable & Sustainable Energy Reviews*, 12 (5) (2008) 1419-1434.

[5] S. C. Ferreira, G. V. Kuik, G. V. Bussel and F. Scarano, Visualization by PIV of dynamic stall on a vertical axis wind turbine, *Experiments in Fluids*, 46 (1) (2008) 97-108.

[6] L. W. Carr, Progress in analysis and prediction of dynamic stall, *J. of Aircraft*, 25 (1) (1988) 6-17.

[7] P. P. Friedmann, M. D. Terlizzi and T. F. Myrtle, New developments in vibration reduction with actively controlled trailing edge flaps, *Mathematical & Computer Modelling*, 33 (10) (2001) 1055-1083.

[8] S. R. Viswamurthy and R. Ganguli, An optimization approach to vibration reduction in helicopter rotors with multiple active trailing edge flaps, *Aerospace Science & Technology*, 8 (3) (2004) 185-94.

[9] C. K. Maucher, B. A. Grohmann, P. Danker, A. Altmikus, F. Jensen and H. Baier, Actuator design for the active trailing edge of a helicopter rotor blade, *Proceedings of the 33rd European Rotorcraft Forum*, Kazan, Russia (2007) 11-13.

[10] A. Mishra, J. Sitaraman, J. D. Baeder and D. G. Opoku, Computational investigation of trailing edge flap for control of vibration, *The 25th AIAA Applied Aerodynamics Conference*, Miami, Florida, USA (2007) 1-25.

[11] E. A. Bossanyi, Individual blade pitch control for load reduction, *Wind Energy*, 6 (2) (2003) 119-28.

[12] T. J. Larsen, H. A. Madsen and K. Thomsen, Active load reduction using individual pitch: based on local blade flow measurements, *Wind Energy*, 8 (1) (2005) 67-80.

[13] T. Buhl, M. Gaunaa and C. Bak, Potential load reduction using airfoils with variable trailing edge geometry, *J. of Solar Energy Engineering*, 127 (4) (2005) 503-516.

[14] T. K. Barlas and G. V. Kuik, Aeroelastic modelling and comparison of advanced active flap control concepts for load reduction on the upwind 5MW wind turbine, *Proceedings of the 2009 European Wind Energy conference & Exhibition*, Marseille, French (2009) 1-12.

[15] I. Abdallah, A*dvanced load alleviation for wind turbines using adaptive trailing edge flaps: sensoring and control*, Denmark Technical University, Roskilde, Denmark (2010).

[16] M. A. Lackner and G. V. Kuik, A comparison of smart rotor control approaches using trailing edge flaps and individual pitch control, *Wind Energy*, 13 (2) (2010) 117-134.

[17] H. Markou, P. B. Andersen and G. C, Larsen, Potential load reductions on megawatt turbines exposed to wakes using individual-pitch wale compensator and trailing-edge flaps, *Wind Energy*, 14 (7) (2011) 841-857.

[18] W. J. Zhu, W. Z. Shen and J. N. Serrensen, Modeling of airfoil trailing edge flap with immersed boundary method, *The 2011 International Conference on Offshore Wind Energy and Ocean Energy*, Beijing, China (2011) 1-9.

[19] T. Lutz, A. Wolf, W. Wiirz and J. G. Jeremiasz, Design and verification of an airfoil with trailing edge flap and unsteady wind tunnel tests, *UPWIND Technical Report*, Stuttgart, Germany (2011).

[20] N. Troldborg, Computational study of the riso airfoil with a hinged flap providing variable trailing edge geometry, *Wind Engineering*, 29 (2) (2005) 89-113.

[21] G. K. Tan, G. X. Shen and W. H. Su, Experimental investigation on the aft-element flapping of a two-element airfoil at high attack angle, *J. of Experiments in Fluid Mechanics*, 21 (3) (2007) 1-7.

[22] Q. Xiao, W. Liu and A. Incecik, Flow control for VATT by fixed and oscillating flap, *Renewable Energy*, 51 (2013) 141-152.

[23] I. Paraschivoiu, *Wind turbine design: with emphasis on darrieus concept*, Polytechnic International Press, Montreal, Canada (2002).

[24] J. C. Hunt, A. A Wray and P. Moin, Eddies stream and convergence zones in turbulent flows, *Proceedings of the 1988 Summer Program*, California, USA (1998) 193-208.

Yang Yang is a Ph.D. candidate at University of Shanghai for Science and Technology. His research area is wind turbine blade design and flow control.

Chun Li is currently a Professor at University of Shanghai for Science and Technology. His research fields include the flow control of wind farm, stall of VAWT and aeroelasticity of wind turbine.